Scientia Iranica A (2013) 20(5), 1401–1414

Sharif University of Technology
Scientia Iranica
Transactions A: Civil Engineering
www.scientiairanica.com

Control volume finite element modeling of free convection inside an inclined porous enclosure with a sinusoidal hot wall

A. Janalizadeh[a], S. Soleimani Kutanaei[a] and E. Ghasemi[b,1,*]

a. *Department of Civil Engineering, Babol University of Technology, Babol, Iran.*
b. *Department of Mechanical Engineering, University of Idaho, 1776 Science Center Dr, Idaho Falls, ID 83402, USA.*

Received 18 August 2012; received in revised form 2 january 2013; accepted 4 February 2013

KEYWORDS
Porous enclosure;
Natural convection;
Sinusoidal wall;
Inclination angle;
CVFEM.

Abstract. In this study, the effects of different governing parameters on natural convection heat transfer between an inclined hot basement roof and a cold environment are investigated numerically, using the Control Volume based Finite Element Method (CVFEM). The medium between the cold and hot surfaces is filled by soil, which can be considered as a porous media. The physical model can be approximated as an enclosure with various inclination angles. The cold wall of the enclosure is assumed to mimic a sinusoidal profile with different dimensionless amplitudes. The numerical investigations are conducted at the Prandtl number (Pr = 1) and various values of non-dimensional governing parameters, namely, the porosity (ε), Darcy number (Da) and Rayleigh number (Ra). The geometrical variables in this study are the inclination angle (γ) and dimensionless amplitude (a) of the sinusoidal cold wall. The obtained results show the significant effects of γ and a on the streamlines and isotherms, as well as the local and average Nusselt numbers at various values of Da, ε and Ra. Effects of the governing parameters on heat transfer and fluid flow in the upper and lower parts of the enclosure are also investigated.

1. Introduction

Natural convective flow in differentially heated enclosures filled with Darcian or non-Darcian fluid-saturated porous media has received considerable attention in the literature. This topic is of practical interest in several sciences, engineering, agriculture, building and geothermal sciences. Nithiarasu et al. [1] examined the effects of variable porosity on convective flow patterns inside a porous cavity. In their study, the flow was triggered by sustaining a temperature gradient between isothermal lateral walls. They found that for the case of a medium with variable porosity, the nature of porosity variation significantly affects heat transfer and flow results. Pakdee and Rattanadecho [2] performed numerical investigations of transient natural convection flow through a fluid-saturated porous medium in a rectangular cavity with a convection surface condition. It was found that the heat transfer coefficient, Rayleigh number and Darcy number considerably influenced characteristics of flow and heat transfer mechanisms. Furthermore, the flow pattern is found to have a local effect on the heat convection rate. Baytas and Pop [3] have studied natural convection on a trapezoidal porous enclosure with situations such as the top enclosure being cooled, the bottom surface being heated and the remaining two non-parallel plane sidewalls of the enclosure being adiabatic. Although

1. *Present address: Department of Mechanical and Material Engineering, Florida International University, Engineering Center, Miami, FL 33174, USA.*
*. *Corresponding author. Tel./Fax: +1 208-533 8157*
E-mail addresses: ghas5622@vandals.uidaho.edu, eghas001@fiu.edu (E. Ghasemi)

their study deals with heat transfer analysis on various application in trapezoidal porous spaces, a comprehensive analysis on heat transfer and flow circulations for applications on the extraction of molten metals, salt water and olive oil confined within a porous bed is yet to appear in literature for various tilt angles.

The geometrical pattern can be useful in improving the heat transfer performance. Natural convection heat transfer inside a wavy enclosure is one of the several devices employed for enhancing the heat and mass transfer efficiency. Flow and heat transfer from irregular surfaces are often encountered in many engineering applications to enhance heat transfer such as micro-electronic devices, flat-plate solar collectors and flat-plate condensers in refrigerators, geophysical applications, electric machinery, cooling system of micro-electronic devices, etc. Saidi et al. [4] presented numerical and experimental results of flow over and heat transfer from a sinusoidal cavity. They reported that the total heat exchange between the wavy wall of the cavity and the flowing fluid was reduced by the presence of a vortex. Das and Mahmud [5] conducted a numerical investigation of natural convection in an enclosure consisting of two isothermal horizontal wavy walls and two adiabatic vertical straight walls. They reported that the amplitude-wavelength ratio affected local heat transfer rate, but it had no significant influence on average heat transfer rate. Adjlout et al. [6] conducted a numerical study on natural convection in an inclined cavity with a hot wavy wall and cold flat wall. One of their interesting findings was the decrease of average heat transfer with the surface waviness, when compared with a flat wall cavity.

The numerical investigation of natural convection in an enclosure with vertical wavy walls was studied by Mahmud et al. [7]. In this work, for a fluid with $\mathrm{Pr} = 0.7$, they simulated the behavior of fluid flow and heat transfer performance for different values of aspect ratio, Grashof number and amplitude-wavelength ratio. They showed that the average heat transfer will decrease with the increase of surface waviness and that a higher heat transfer rate is observed at lower aspect ratios for a certain value of Grashof number. Yao [8] has studied theoretically the natural convection along a vertical wavy surface. He found that the heat transfer rate for a wavy surface was constantly smaller than that of a corresponding flat plate. The influence of the geometrical parameters on the mean Nusselt number is clearly shown from his results. Dalal and Das [9] analyzed numerically the natural convection in a cavity with a wavy wall heated from below. Their results showed that the presence of undulation in the right wall affected local heat transfer rate and flow field, as well as thermal field. Rostami [10] investigated the unsteady heat transfer and fluid flow characteristics in an enclosure with two vertical wavy and two horizontal straight walls. Simulation was carried out for different values of Grashof number, Prandtl number, wave ratio and aspect ratio.

Kumar [11] analyzed numerically, using the finite element method, the free convection induced by a vertical wavy surface with uniform heat flux in a porous enclosure. The results revealed that small sinusoidal drifts from the smoothness of a vertical wall with a phase angle of 60° and high frequency enhanced the free convection from a vertical wall with uniform heat flux. Chen et al. [12] analyzed numerically the steady-state free convection inside a cavity made of two horizontal straight walls and two vertical bent-wavy walls filled with a fluid-saturated porous medium. Their results showed that the dependence of the local Nusselt number on Darcy number and porosity was not small at large Darcy-Rayleigh numbers. Ghasemi et al. [13] studied the steady two-dimensional laminar forced magneto-hydrodynamic Hiemenz flow against a flat plate with variable wall temperature in a porous medium [14-16] analytically by means of the homotopy analysis method (HAM) [17-20]. It was found that increments in the suction/injection parameter, the Hartmann number and the permeability parameter increase the velocity profiles but decrease the temperature profiles. Contrarily, increments in the Prandtl number decrease the velocity profiles and increase the temperature profiles.

The main objective of the present work is to conduct a numerical investigation of natural convection heat transfer in an enclosure with one cold sinusoidal wall at different inclination angles and dimensionless amplitude of the cold wall, using the Control Volume based Finite Element Method (CVFEM) [21-24].

Control Volume based Finite Element Method (CVFEM) is a scheme that uses the advantages of both finite volume [25-28] and finite element methods for simulation of multi-physics problems in complex geometries

The numerical investigation is carried out for different governing parameters such as the Rayleigh number, Darcy number, porosity and the inclination angle of the enclosure.

2. Geometry definition and boundary conditions

The physical model along with the important geometrical parameters and the mesh of the enclosure used in the present CVFEM program are shown in Figure 1. The enclosure has a width/height aspect ratio of two. The two sidewalls with length H are thermally insulated, whereas the lower flat and upper sinusoidal walls are maintained at constant temperatures T_h and T_c, respectively. Under all circumstances, $T_h > T_c$ condition is maintained. The shape of the upper

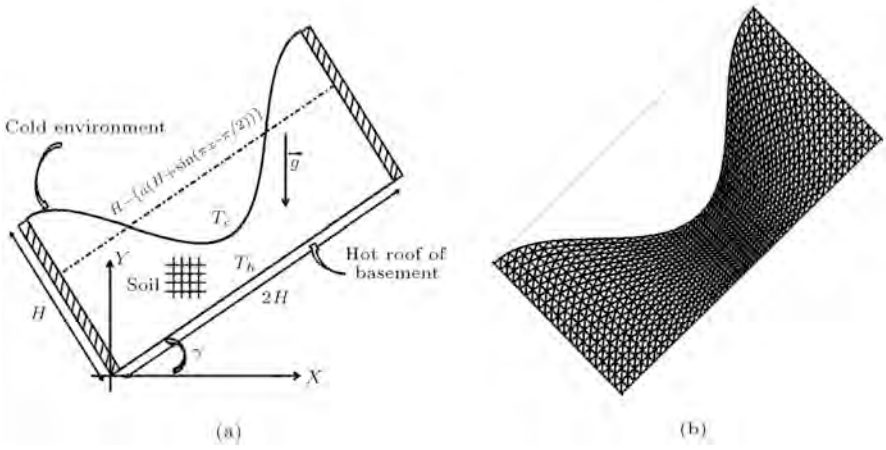

Figure 1. (a) Geometry and boundary conditions with (b) the mesh of enclosure considered in this work.

sinusoidal wall profile is assumed to mimic the following pattern:

$$Y = H - \{a(H + \sin(\pi x - \pi/2))\}, \tag{1}$$

where a is the dimensionless amplitude of the sinusoidal wall. The above geometry could be considered as heat transfer between the roof of a basement and a cold environment.

3. Mathematical modeling and numerical procedure

3.1. Problem formulation

The porous medium is assumed to be homogeneous and thermally isotropic and saturated with a fluid that is in local thermodynamic equilibrium with the solid matrix. The fluid flow is laminar and incompressible. The pressure work and viscous dissipation are all assumed negligible. The thermo physical properties of the porous medium are taken to be constant. However, the Boussinesq approximation takes into account the effect of density variation on the buoyancy force. Furthermore, the solid matrix is made of spherical particles, while the porosity and permeability of the medium are assumed to be uniform throughout the enclosure. Using standard symbols, the governing equations describing the heat transfer phenomenon are given by:

$$\frac{\partial u}{\partial x} + \frac{\partial v}{\partial y} = 0, \tag{2}$$

$$\frac{1}{\varepsilon}\frac{\partial u}{\partial t} + \frac{u}{\varepsilon^2}\frac{\partial u}{\partial x} + \frac{v}{\varepsilon^2}\frac{\partial u}{\partial y} = -\frac{1}{\rho_f}\frac{\partial P}{\partial x} + \frac{\upsilon}{\varepsilon}\left(\frac{\partial^2 u}{\partial x^2} + \frac{\partial^2 u}{\partial y^2}\right) - \frac{\mu u}{\rho_f k}, \tag{3}$$

$$\frac{1}{\varepsilon}\frac{\partial v}{\partial t} + \frac{u}{\varepsilon^2}\frac{\partial v}{\partial x} + \frac{v}{\varepsilon^2}\frac{\partial v}{\partial y} = -\frac{1}{\rho_f}\frac{\partial P}{\partial y} + \frac{\upsilon}{\varepsilon}\left(\frac{\partial^2 v}{\partial x^2} + \frac{\partial^2 v}{\partial y^2}\right) + g\beta(T - T_\infty) - \frac{\mu v}{\rho_f k}, \tag{4}$$

$$\sigma\frac{\partial T}{\partial t} + u\frac{\partial T}{\partial x} + v\frac{\partial T}{\partial y} = \alpha\left(\frac{\partial^2 T}{\partial x^2} + \frac{\partial^2 T}{\partial y^2}\right), \tag{5}$$

$$\sigma = \frac{[\varepsilon(\rho C_p)_f + (1-\varepsilon)(\rho C_p)_s]}{(\rho C_p)_f}, \tag{6}$$

where k is medium permeability, β is thermal expansion coefficient, α is effective thermal diffusivity of the porous medium, μ and υ are viscosity and kinematic viscosity of the fluid, respectively. In the present study, the heat capacity ratio, σ, is taken to be unity, since the thermal properties of the solid matrix and the fluid are assumed identical. The momentum equation consists of the Brinkmann term, which accounts for viscous effects due to the presence of the solid body [29]. This form of momentum equation is known as the Brinkmann-extended Darcy model. Lauriat and Prasad [30] employed the Brinkmann-extended Darcy formulation to investigate the buoyancy effects on natural convection in a vertical enclosure. Although the viscous boundary layer in the porous medium is very thin for most engineering applications, inclusion of this term is essential for heat transfer calculations [31]. However, the inertial effect was neglected, as the flow was relatively low. The variables are transformed into the dimensionless quantities defined as:

$$X = \frac{x}{L}, \quad Y = \frac{y}{L}, \quad \tau = \frac{t\alpha}{H^2}, \quad U = \frac{uH}{\alpha}, \quad V = \frac{uH}{\alpha}, \quad \Omega = \frac{\omega H^2}{\alpha}, \quad \Psi = \frac{\psi}{\alpha}, \quad \Theta = \frac{T - T_c}{T_h - T_c}, \tag{7}$$

where ω and ψ represent dimensional vorticity and stream function, respectively. Symbol α denotes thermal diffusivity.

$$\frac{\partial^2\Psi}{\partial X^2}+\frac{\partial^2\Psi}{\partial Y^2}=-\Omega, \tag{8}$$

$$\varepsilon\frac{\partial\Omega}{\partial t}+\frac{\partial\Psi}{\partial Y}\frac{\partial\Omega}{\partial X}-\frac{\partial\Psi}{\partial X}\frac{\partial\Omega}{\partial Y}=\varepsilon\mathrm{Pr}\left(\frac{\partial^2\Omega}{\partial X^2}+\frac{\partial^2\Omega}{\partial Y^2}\right)+\mathrm{RaPr}\varepsilon^2\left(\frac{\partial\Theta}{\partial X}\right)-\frac{\mathrm{Pr}\varepsilon^2}{\mathrm{Da}}\Omega, \tag{9}$$

$$\sigma\frac{\partial\Theta}{\partial t}+\frac{\partial\Psi}{\partial Y}\frac{\partial\Theta}{\partial X}-\frac{\partial\Psi}{\partial X}\frac{\partial\Theta}{\partial Y}=\alpha\left(\frac{\partial^2\Theta}{\partial X^2}+\frac{\partial^2\Theta}{\partial Y^2}\right), \tag{10}$$

where the Darcy number, Da, is defined as k/H^2, and $\mathrm{Pr}=v/\alpha$ is a Prandtl number where $\alpha=k_e/(\rho C_p)_f$ is the thermal diffusivity. The Rayleigh number, Ra, is defined as:

$$\mathrm{Ra}=g\beta L^3(T_h-T_c)/(\alpha v).$$

The boundary conditions as shown in Figure 1 are:

$$\begin{array}{ll}\Theta=1.0 & \text{on the hot wall,}\\ \Theta=0.0 & \text{on the cold wall,}\\ \partial\Theta/\partial n=0.0 & \text{on the two other insulation boundaries,}\\ \Psi=0.0 & \text{on all solid boundaries.}\end{array} \tag{11}$$

The values of vorticity on the boundary of the enclosure can be obtained using the stream function formulation and the known velocity conditions during the iterative solution procedure. The local Nusselt number along the hot wall can be expressed as:

$$\mathrm{Nu}_{\mathrm{loc}}=\left.\frac{\partial\Theta}{\partial x}\right|_{\text{hot wall}}. \tag{12}$$

The average Nusselt number on the hot wall is evaluated as:

$$\mathrm{Nu}_{\mathrm{ave}}=\frac{1}{2H}\int_0^{\gamma}\mathrm{Nu}_{\mathrm{local}}(x)dx. \tag{13}$$

3.2. Numerical procedure

Triangular elements are considered as the building block of the discretization, using CVEM. The values of variables are approximated with linear interpolation within the elements. A control volume is created by joining the center of each element in the support to the mid points of the element sides that pass through the central node i, which creates a close polygonal control volume (see Figure 1(b)).

To illustrate the solution procedure, using the CVFEM, one can consider the general form of advection-diffusion equation for node i in integral form:

$$-\int_V QdV-\int_A k\nabla\phi\cdot ndA+\int_A(v\cdot n)\phi dA=0, \tag{14}$$

or point form:

$$-\nabla\cdot(k\nabla\phi)+\nabla\cdot(v\phi)-Q=0, \tag{15}$$

which can be represented by the system of CVFEM discrete equations as:

$$[a_i+Qc_i+Bc_i]\,\phi_i=\sum_{j=1}^{n_i}a_{i,j}\phi_{S_{i,j}}+Q_{B_i}+B_{B_i}. \tag{16}$$

In the above equation, the a's are the coefficients, the index (i,j) indicates the jth node in the support of node i, the index $S_{i,j}$ provides the node number of the jth node in the support, the B's account for boundary conditions and the Q's for source terms. For the selected triangular element which is shown in Figure 2, this approximation without considering the source term leads to:

$$-(a_1^k+a_1^u)\phi_i+(a_2^k+a_2^u)\phi_{S_{i,3}}+(a_2^k+a_2^u)\phi_{S_{i,4}}=0. \tag{17}$$

By the upwinding, advective coefficients, identified with the superscripts $()^u$, are given by:

$$\begin{aligned}a_1^u&=\max[q_{f1},0]+\max[q_{f2},0],\\ a_2^u&=\max[-q_{f1},0],\\ a_3^u&=\max[-q_{f2},0].\end{aligned} \tag{18}$$

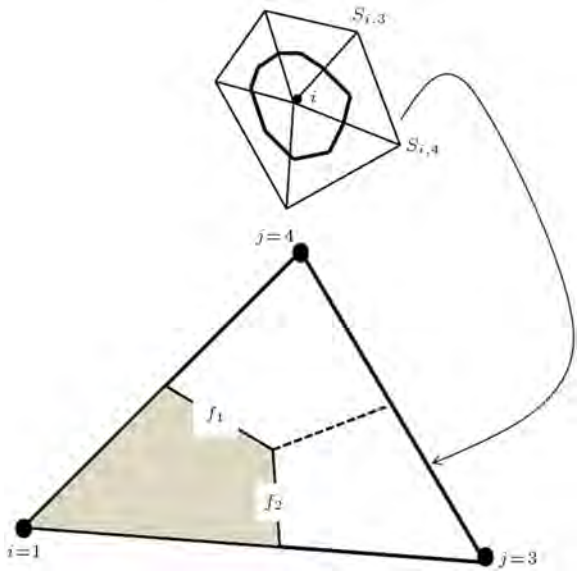

Figure 2. A sample triangular element and its corresponding control volume.

And the diffusion coefficients, identified with the superscripts $()^k$, are given by:

$$\begin{aligned} a_1^k =& -k_{f1}N_{1x}\Delta\vec{y}_{f1} + k_{f1}N_{1y}\Delta\vec{x}_{f1} \\ & - k_{f2}N_{1x}\Delta\vec{y}_{f2} + k_{f2}N_{1y}\Delta\vec{x}_{f2}, \\ a_2^k =& -k_{f1}N_{2x}\Delta\vec{y}_{f1} + k_{f1}N_{2y}\Delta\vec{x}_{f1} \\ & - k_{f2}N_{2x}\Delta\vec{y}_{f2} + k_{f2}N_{2y}\Delta\vec{x}_{f2}, \\ a_2^k =& -k_{f1}N_{3x}\Delta\vec{y}_{f1} + k_{f1}N_{3y}\Delta\vec{x}_{f1} \\ & - k_{f2}N_{3x}\Delta\vec{y}_{f2} + k_{f2}N_{3y}\Delta\vec{x}_{f2}. \end{aligned} \tag{19}$$

In Eq. (15), the volume flow across face 1 and 2 in the direction of the outward normal is:

$$\begin{aligned} q_{f1} &= v \cdot n.A\big|_{f1} = v_x^{f1}\Delta\vec{y}_{f1} - v_y^{f1}\Delta\vec{y}_{f1}, \\ q_{f2} &= v \cdot n.A\big|_{f2} = v_x^{f2}\Delta\vec{y}_{f2} - v_y^{f2}\Delta\vec{y}_{f2}. \end{aligned} \tag{20}$$

The value of the diffusivity at the mid-point of face 1 can be obtained as:

$$k_{f1} = [N_1k_1 + N_2k_2 + N_3k_3]_{f1} = \frac{5}{12}k_1 + \frac{5}{12}k_2 + \frac{2}{12}k_3, \tag{21}$$

and at the mid-point of face 2:

$$k_{f2} = [N_1k_1 + N_2k_2 + N_3k_3]_{f2} = \frac{5}{12}k_1 + \frac{2}{12}k_2 + \frac{5}{12}k_3. \tag{22}$$

The velocity components at the midpoint of face 1 are:

$$\begin{aligned} v_x^{f1} &= \frac{5}{12}v_{x_1} + \frac{5}{12}v_{x_2} + \frac{2}{12}v_{x_3}, \\ v_y^{f1} &= \frac{5}{12}v_{y_1} + \frac{5}{12}v_{y_2} + \frac{2}{12}v_{y_3}. \end{aligned} \tag{23}$$

And on face 2:

$$\begin{aligned} v_x^{f2} &= \frac{5}{12}v_{x_1} + \frac{2}{12}v_{x_2} + \frac{5}{12}v_{x_3}, \\ v_y^{f2} &= \frac{5}{12}v_{y_1} + \frac{2}{12}v_{y_2} + \frac{5}{12}v_{y_3}. \end{aligned} \tag{24}$$

These values can be used to update the ith support coefficients through the following equation:

$$\begin{aligned} a_i &= a_i + a_1^k, \\ a_{i,3} &= a_{i,3} + a_2^k, \\ a_{i,4} &= a_{i,4} + a_3^k. \end{aligned} \tag{25}$$

In Eq. (18), moving counter-clockwise around node i, the signed distances are:

$$\begin{aligned} \Delta\vec{x}_{f1} &= \frac{x_3}{3} - \frac{x_2}{6} - \frac{x_1}{6}, \\ \Delta\vec{x}_{f2} &= -\frac{x_2}{3} + \frac{x_3}{6} + \frac{x_1}{6}, \\ \Delta\vec{y}_{f1} &= \frac{y_3}{3} - \frac{y_2}{6} - \frac{y_1}{6}, \\ \Delta\vec{y}_{f2} &= -\frac{y_2}{3} + \frac{y_3}{6} + \frac{y_1}{6}. \end{aligned} \tag{26}$$

The derivatives of the shape functions are:

$$\begin{aligned} N_{1x} &= \frac{\partial N_1}{\partial x} = \frac{(y_2 - y_3)}{2V^{\text{ele}}}, \\ N_{1y} &= \frac{\partial N_1}{\partial y} = \frac{(x_3 - x_2)}{2V^{\text{ele}}}, \\ N_{2x} &= \frac{\partial N_2}{\partial x} = \frac{(y_3 - y_1)}{2V^{\text{ele}}}, \\ N_{2y} &= \frac{\partial N_1}{\partial y} = \frac{(x_1 - x_3)}{2V^{\text{ele}}}, \\ N_{3x} &= \frac{\partial N_2}{\partial x} = \frac{(y_1 - y_2)}{2V^{\text{ele}}}, \\ N_{3y} &= \frac{\partial N_3}{\partial y} = \frac{(x_2 - x_1)}{2V^{\text{ele}}}, \end{aligned} \tag{27}$$

and the volume of the element is:

$$V^{\text{ele}} = \frac{(x_2y_3 - x_3y_2) + x_1(y_2 - y_3) + y_1(x_3 - x_2)}{2}. \tag{28}$$

The obtained algebretic equations from the discretization procedure, using CVFEM, are solved by the Gauss-Seidel Method.

3.3. Implementation of source terms and boundary conditions

The boundary conditions for the present problem can be enforced using B_{B_i} and B_{C_i} as follows:

Insulated boundary:

$$B_{B_i} = 0 \qquad \text{and} \qquad B_{C_i} = 0, \tag{29}$$

Insulated boundary:

$$B_{B_i} = 0 \qquad \text{and} \qquad B_{C_i} = 0, \tag{30}$$

Fixed value boundary:

$$B_{B_i} = \phi_{value} \times 10^{16} \qquad \text{and} \qquad B_{C_i} = 10^{16}, \tag{31}$$

Table 1. Comparison of the average Nusselt number Nu_{ave} for different grid resolutionat $Ra = 10^5$, $Da = 0.1$ and $\varepsilon = 0.5$; $\gamma = 90^\circ$ and $Pr = 1$.

Mesh size								
21 × 41	31 × 61	41 × 81	51 × 101	61 × 121	71 × 141	81 × 161	91 × 181	101 × 201
3.176	3.374	3.460	3.503	3.527	3.543	3.552	3.558	3.563

where ϕ_{value} is the prescribed value on the boundary, and A_k is the length of the control volume surface on the boundary segment. The volume source terms can be applied to Eq. (16) as:

$$\sum_{j=1}^{elements} \int_{V_j} Q dV \approx Q_i V_i, \tag{32}$$

or after linearizing the source term:

$$Q_i V_i = -Q_{C_i} \phi_i + Q_{B_i}. \tag{33}$$

4. Grid tsting and code validation

A mesh testing procedure was conducted to guarantee the grid-independency of the present solution. Various mesh combinations were explored for the case of $Ra = 10^5$, $Da = 0.1$, $\varepsilon = 0.5$ and $\gamma = 90^\circ$ for Prandtl number ($Pr = 1$), as shown in Table 1. The present code was tested for grid independence by calculating the average Nusselt number on the inner hot wall. In harmony with this, it was found that a grid size of 71 × 141 ensures a grid-independent solution. The convergence criterion for the termination of all computations is:

$$\max_{grid} \left|\Gamma^{n+1} - \Gamma^n\right| \leq 10^{-7}, \tag{34}$$

where n is the iteration number, and Γ stands for the independent variables (Ω, Ψ, Θ). To validate the present study, the results obtained, using the CVFEM code, are compared for $Pr = 0.7$ with other works reported in [32,33], as seen in Table 2. Table 3 illustrates the comparison between the calculated average Nusselt numbers of Nithiarasu et al. [1]. These comparisons illustrate an excellent agreement between the present calculations and the previous works.

Table 2. Comparison of the present results with previous works for different Rayleigh numbers when $Pr = 0.7$.

Ra	Present	Khanafer et al. [32]	De Vahl Davis [33]
10^3	1.1432	1.118	1.118
10^4	2.2749	2.245	2.243
10^5	4.5199	4.522	4.519

Table 3. Comparison of the present results with previous works for different Rayleigh numbers when $Pr = 1$.

Ra	$\varepsilon = 0.4$		$\varepsilon = 0.6$	
	Present	Nithiarasu et al. [1]	Present	Nithiarasu et al. [1]
10^3	1.0199	1.01	1.0249	1.015
10^4	1.4222	1.418	1.5571	1.530
10^5	3.1674	3.083	3.6497	3.595

5. Results and Discussion

Numerical simulations of natural convection flow through a fluid-saturated porous medium in an enclosure with one sinusoidal wall were performed. Effects of the dimensionless amplitude of the sinusoidal wall, Rayleigh number, porosity, Darcy number and inclination angle of the enclosure on the heat transfer and fluid flow are shown in terms of streamlines and isotherms. The heat transfer characteristic from the straight hot wall is investigated using the average and local Nusselt numbers. Figure 3 shows the effect of dimensionless amplitude (a) of the sinusoidal wall, along with the inclination angle (γ) on the isotherms and streamlines at $Da = 10^{-3}$, $\varepsilon = 0.5$ and $Ra = 10^3$. For all inclination angles, the temperature distribution and temperature contours are uniformly distributed, and isothermal lines are nearly parallel to each other following the geometry of the sinusoidal surfaces; this shows the characteristic of the conduction dominant mechanism of heat transfer at low Rayleigh numbers. At $\gamma = 0^\circ$ two counter rotating vortices are observed. This bicellular flow pattern divides the enclosure into two symmetric parts, with respect to the vertical centerline of the enclosure. An increase of a for this inclination angle results in stronger circulation in the enclosure because of the decrement of distance between the hot and cold walls. As seen in Figure 3, the effect of enclosure wall amplitude on the streamline is more pronounced at $\gamma = 45^\circ$ and 90°, while this effect is negligible on the temperature distribution contours at $\gamma = 0^\circ$. At $\gamma = 45^\circ$, a single vortex is formed within the enclosure for $a = 0.1$ and 0.2. From the streamlines, it can be seen that an increase of a from 0.1 to 0.2 causes the center cell of the vortex to move upward. Afterward, as a enhances further up to 0.3, this single cell divides into two cells with different strengths; a

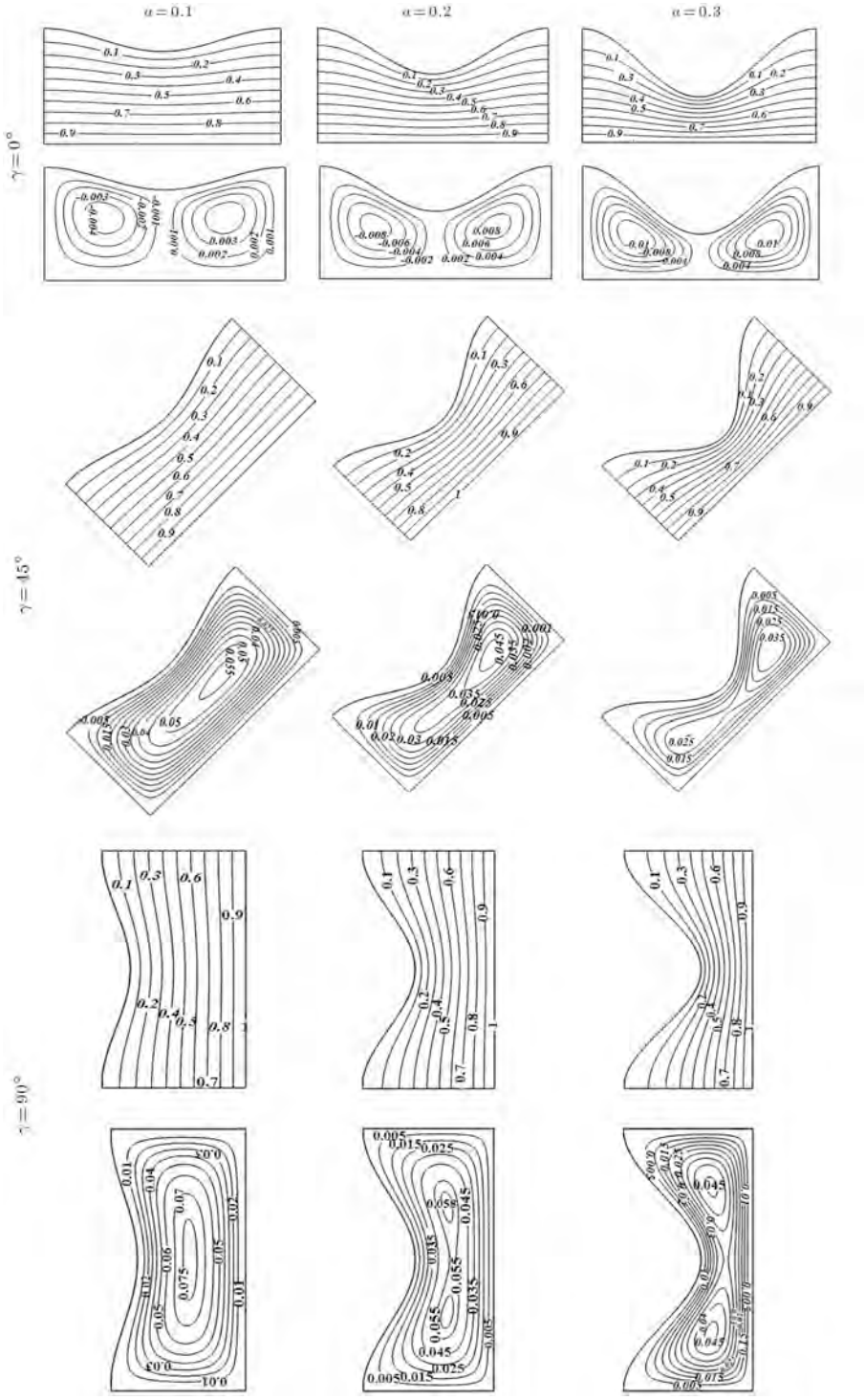

Figure 3. Isotherms (up) and streamlines (down) contours for different values of dimensionless amplitude (a) and inclination angle (γ) at Da = 0.001, $\varepsilon = 0.5$ and Ra = 10^3.

stronger cell in the upper region and a weaker cell in the lower region of the enclosure. However, at $\gamma = 90°$ the division of the main cell into two vortices with equal sizes and strength occurs at $a = 0.2$. It is worthwhile mentioning that contrary to $\gamma = 0°$, an increment of a at $\gamma = 45°$ and $90°$ decreases the strength of vortexes inside the enclosure, because the sinusoidal wall suppresses the flow circulation for these inclination angles.

In Figure 4, the effects of a and γ are investigated for a high Rayleigh number, i.e. Ra = 10^5. In general, as the Rayleigh number increases up to 10^5, the buoyancy-driven circulations inside the enclosure become stronger, as seen from the greater magnitudes

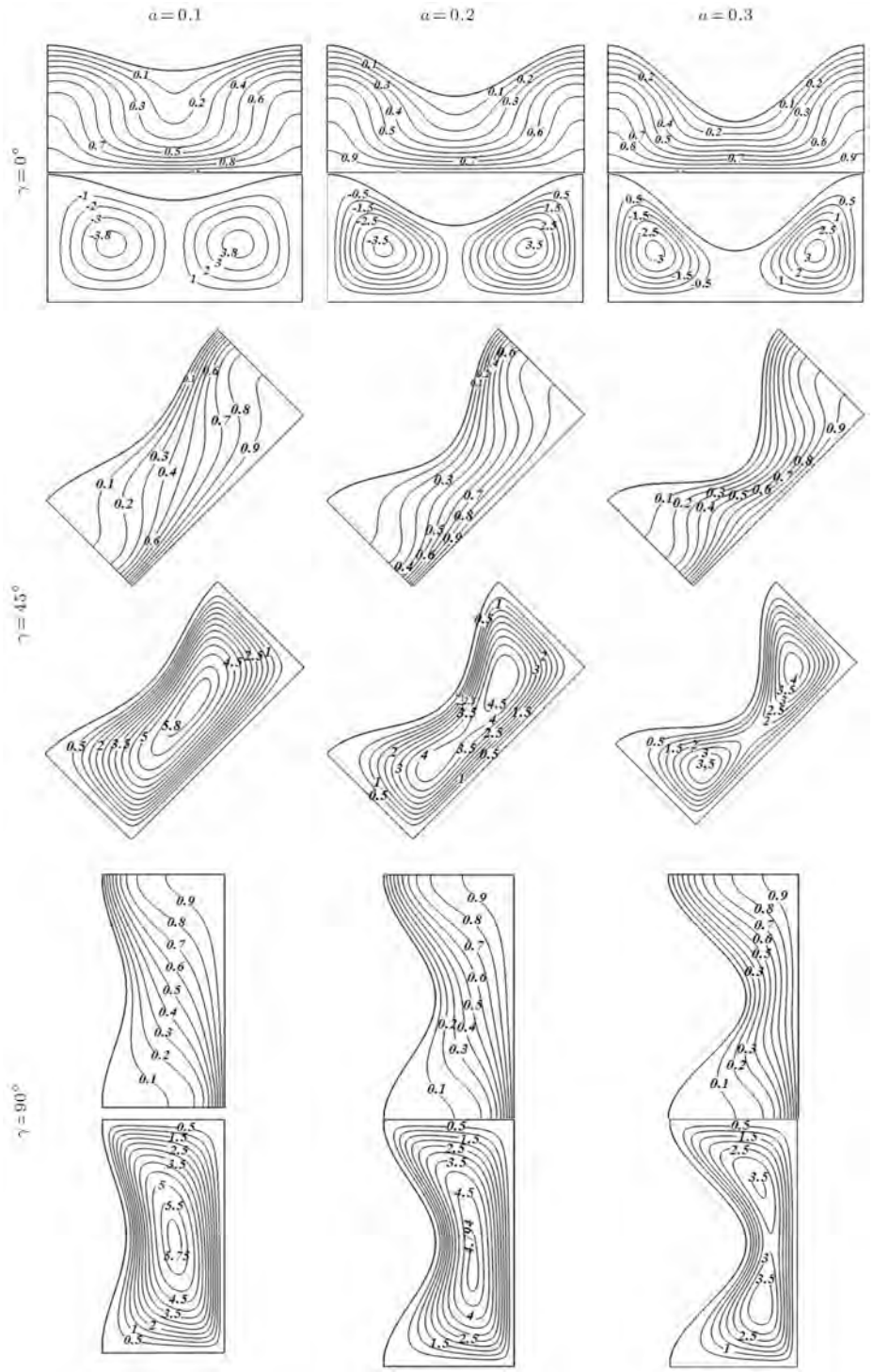

Figure 4. Isotherms (up) and streamlines (down) contours for different values of dimensionless amplitude (a) and inclination angle (γ) at Da = 0.001, $\varepsilon = 0.5$ and Ra = 10^5.

of stream function. In addition, more distortion appears in the isothermal lines. The figure also displays that at $\gamma = 0°$, an increase in a decreases the intensity of the two counterclockwise vortices. This finding is in contrast with the previous result for Ra = 10^3, which may be due to the domination of the conduction mechanism at this Rayleigh number as the distance between the hot and cold walls reduces. The magnitude of the stream function also illustrates that for $\gamma = 45°$, the upper cell for $a = 0.2$ and 0.3 is stronger than that of the lower one (at the bottom), whereas at $\gamma = 90°$, an opposite trend is observed. The isotherms for $\gamma = 45°$ and 90° show that the thermal boundary layer in the vicinity of the hot wall in the upper region

of the enclosure is thinner at $\gamma = 45°$, compared to $\gamma = 90°$, and it is thicker at $\gamma = 90°$ in the lower region of the enclosure. It should be noted that the thermal boundary layer thickness in these regions is related to the intensity of two existent vortices; as stated above, at $\gamma = 45°$, the upper vortex is stronger than that of $\gamma = 90°$. A similar justification could be adopted for the boundary layer at the lower part of the enclosure where the thermal boundary layer is thinner than that of $\gamma = 45°$.

Effects of the Darcy number on the fluid flow and temperature inside the enclosure are depicted in Figure 5. For this case, the effect of Darcy number is investigated at different dimensionless amplitudes (a) and Darcy number (Da), and at a fixed inclination angle of enclosure ($\gamma = 90°$), porosity $\varepsilon = 0.5$ and $\mathrm{Ra} = 10^5$. The streamlines and isotherms are depicted for Darcy numbers $\mathrm{Da} = 10^{-1}$, 10^{-3} and 10^{-5} where the dimensionless amplitude varies from 0.1 to 0.3. From the definition of Darcy number, the direct proportion of the Darcy number to the permeability is clear. The permeability in porous medium works to measure the flow strength and can be considered as conductivity for a fluid flow. Hence, high permeability causes the strong flow circulation in the enclosure, whereas low permeability inhibits the flow circulation inside the enclosure. Comparison of the isotherms shows that for a higher Darcy number, the convection heat transfer inside the enclosure decreases, whereas the conduction is the main heat transfer mechanism at low Darcy numbers. As a result, the isothermal contours are more distorted at high Darcy numbers, while they follow the form of the enclosure at low Darcy numbers. Figure 5 also displays that the dimensionless amplitude of the sinusoidal wall of the enclosure has a significant effect on the flow characteristic inside the enclosure. This influence is completely obvious even at low Darcy numbers in which the the main heat transfer mechanism is conduction. The streamline for different Darcy numbers indicate that the division of the main cell into two vortices occurs when $a = 0.2$ at $\mathrm{Da} = 10^{-5}$, while this division corresponds to $a = 0.3$ at higher Darcy numbers, i.e. $\mathrm{Da} = 10^{-3}$ and 10^{-1}.

The influence of porosity (ε) along with the effect of dimensionless amplitude is reported in Figure 6 for $\gamma = 90°$, $\mathrm{Da} = 10^{-3}$ and $\mathrm{Ra} = 10^5$. As a general observation, the effect of various porosity values on the streamlines and isotherms are less significant, in comparison with the effect of other governing parameters such as Darcy or Rayleigh numbers. From this figure, it is clear that for higher porosity, the drag terms are less significant, leading to greater dimensionless flow velocities. Hence, increase of ε results in higher flow circulation inside the enclosure and a greater magnitude of stream function. In addition, the effect of

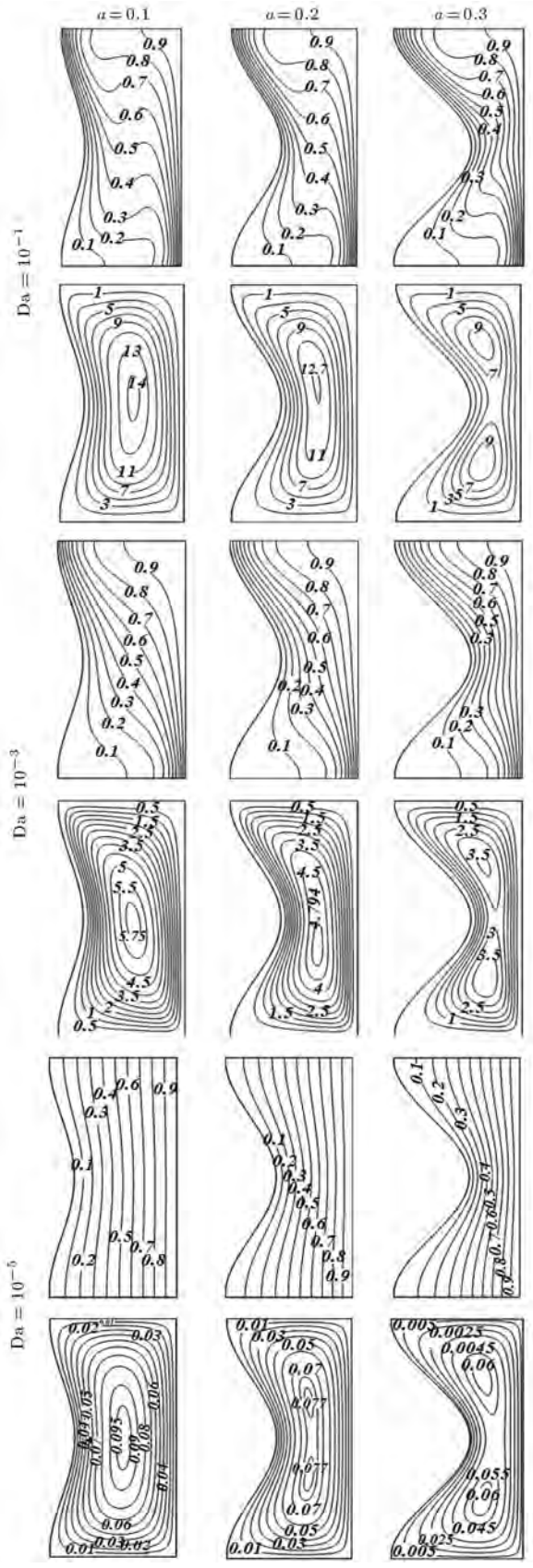

Figure 5. Isotherms (up) and streamlines (down) contours for different values of dimensionless amplitude (a) and Darcy number (Da) at $\gamma = 90$, $\varepsilon = 0.5$ and $\mathrm{Ra} = 10^5$.

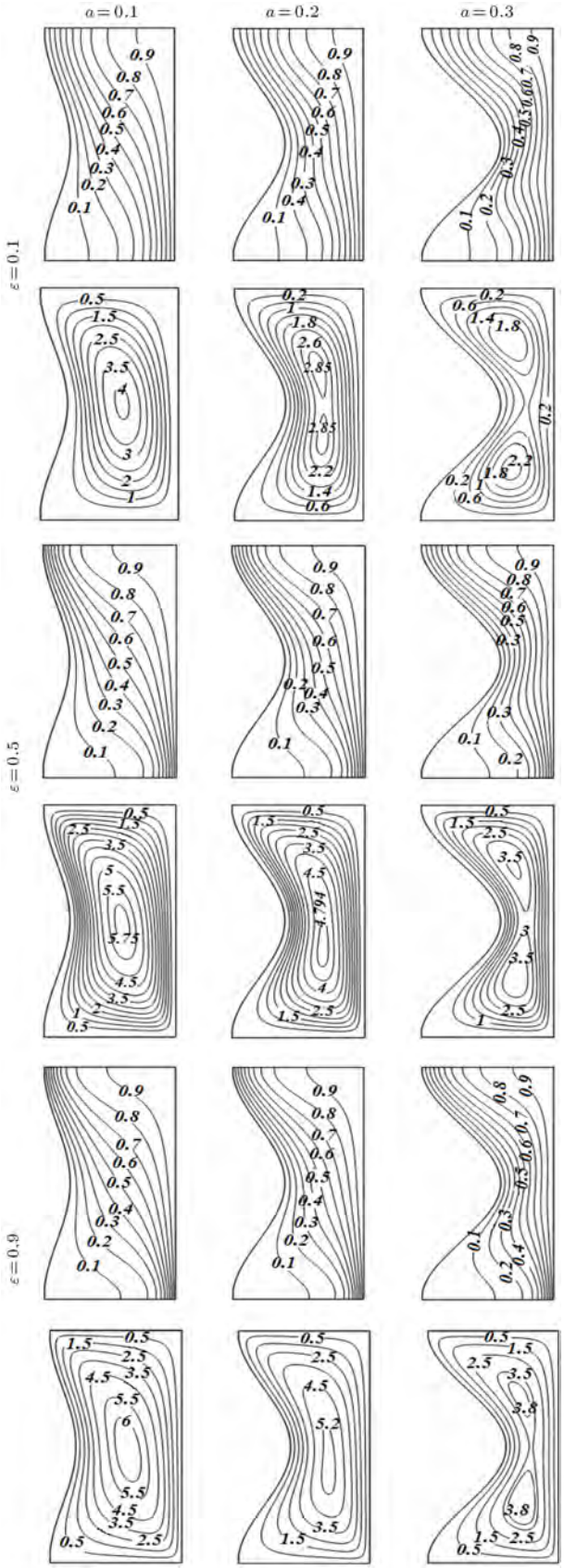

Figure 6. Isotherms (up) and streamlines (down) contours for different values of dimensionless amplitude (a) and porosity (ε) at $\gamma = 90°$, Da = 0.001 and Ra = 10^5.

ε on the isotherm is the same as that of on the increase of Ra.

The distribution of local Nusselt number on the hot wall is depicted in Figures 7 to 10. Figure 7 shows the effect of the inclination angle and Rayleigh number on the local Nusselt number for Da = 10^{-3}, $\varepsilon = 0.5$ and $a = 0.3$. The figure shows that the inclination of the enclosure has no significant effect on the local Nusselt number, which is symmetric with respect to the vertical center line of the enclosure; this is due to the domination of the conduction heat transfer mechanism where the buoyancy forces and therefore the effect of inclination angle is negligible.

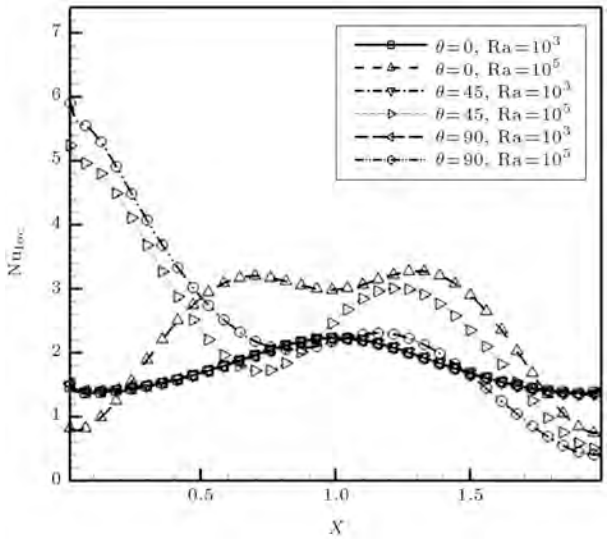

Figure 7. Effects of the Rayleigh number and inclination angle on local Nusselt number at Da = 0.001, $\varepsilon = 0.5$ and $a = 0.3$.

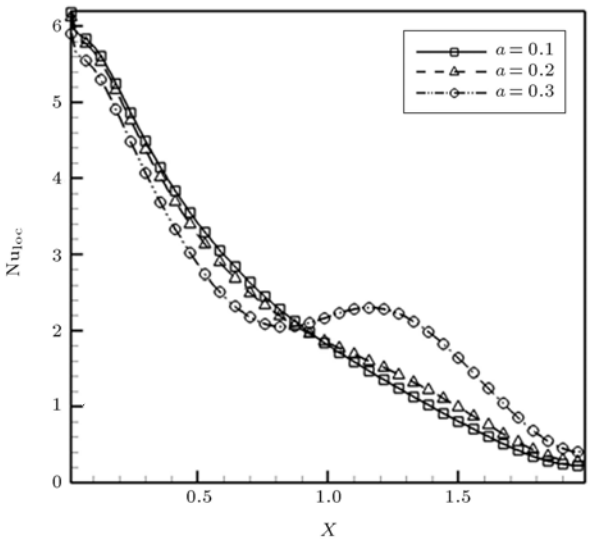

Figure 8. Effects of the dimensionless amplitude on the local Nusselt number at Da = 0.001, $\varepsilon = 0.5$, Ra = 10^5 and $\gamma = 90°$.

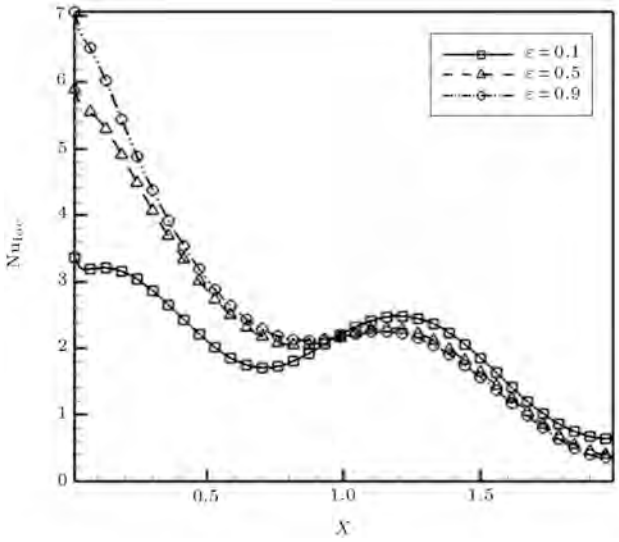

Figure 9. Effects of the porosity on the local Nusselt number at Da = 0.001, $a = 0.3$, Ra = 10^5 and $\gamma = 90°$.

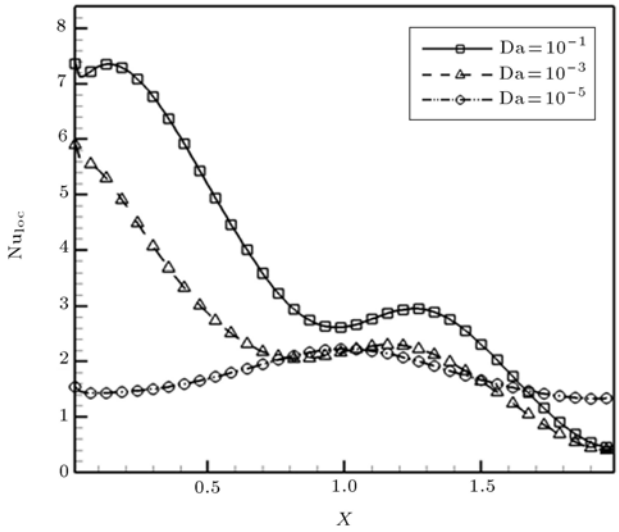

Figure 10. Effects of the Darcy number on the local Nusselt number at $\varepsilon = 0.5$, $a = 0.3$, Ra = 10^5 and $\gamma = 90°$.

For Ra = 10^5 at $\gamma = 90°$, the Nu_{loc} is again symmetric because of the symmetry of the geometry and boundary conditions with respect to the enclosure's centerline. Given this Rayleigh number for $\gamma = 45°$ and 90°, the local Nusselt number is greater at the lower part of the enclosure where the isotherms become denser due to the returning flow accompanying the cold fluid. It is worthwhile mentioning that the local Nusselt number in the lower part of the enclosure is greater for $\gamma = 90°$, in comparison with $\gamma = 45°$, while an opposite trend is seen at the upper part of the enclosure. It may be in correspondence with the strength of the upper and lower vortices for these cases, as stated and discussed in Figure 4.

Figure 8 shows the effects of the dimensionless amplitude on the local Nusselt number at Da = 0.001, $\varepsilon = 0.5$, Ra = 10^5 and $\gamma = 90°$. As seen, when a decreases, the local Nusselt number profile becomes monotonous, whereas the profile experiences a peak near the center of the enclosure for higher values of a.

Effects of the porosity on the local Nusselt number at Da = 0.001, $a = 0.3$, Ra = 10^5 and $\gamma = 90°$ are shown in Figure 9. The general trend of the local Nusselt number is the same for various values of ε, and the increase of the porosity enhances the maximum value of the local Nusselt number. Figure 10 illustrates the effect of Darcy number on the Nu_{loc} at $\varepsilon = 0.5$, $a = 0.3$, Ra = 10^5, and $\gamma = 90°$. As stated previously, an increase in Darcy number makes the convection heat transfer mechanism more pronounced; hence the values of local Nusselt number on the straight heated wall increase.

Figures 11 to 13 display the effect of governing parameters on the average Nusselt number on the heated wall. Figure 11 indicates that at low Rayleigh number (Ra = 10^3), the inclination angle of the enclosure has no significant effect on the average Nusselt number. The figure also indicates that for this case, the effect of (γ) on the Nu_{ave} at Ra = 10^4 is in contrast with that of Ra = 10^5; for Ra = 10^5, the average Nusselt number increases with decrement of inclination angle while it is vice versa for Ra = 10^4. Figure 12 demonstrates the effect of porosity and Darcy numbers on the average Nusselt number at $\gamma = 90°$, $a = 0.2$ and Ra = 10^5. It can be seen that increasing the porosity enhances the Nu_{ave} especially at greater Darcy numbers.

Figure 13 compares the effect of different values of a on the Nusselt number; as a enhances, the magnitude of Nu_{ave} decreases due to the increase of

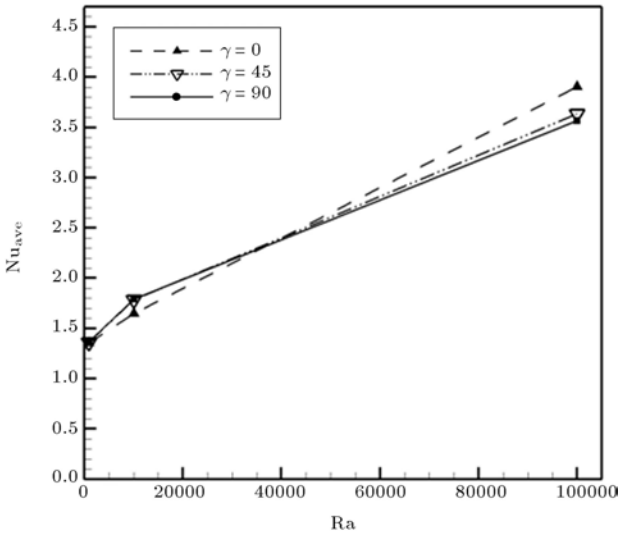

Figure 11. Effects of Ra and γ on the average Nusselt number at $\varepsilon = 0.5$, $a = 0.2$, Da = 0.1.

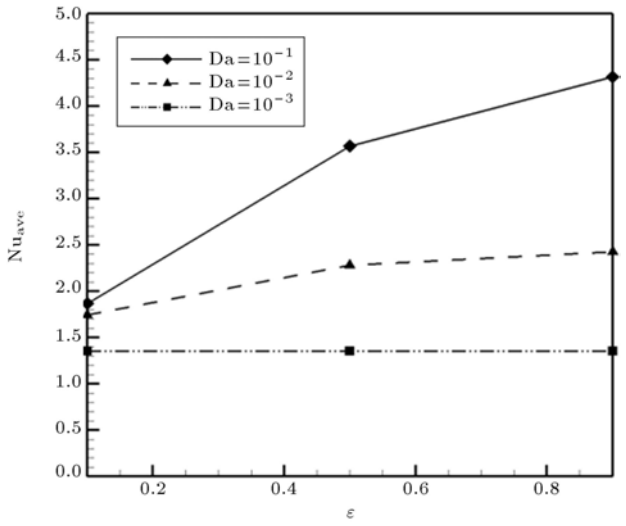

Figure 12. Effects of ε and Da on the average Nusselt number at $\gamma = 90°$, $a = 0.2$, Ra $= 10^5$.

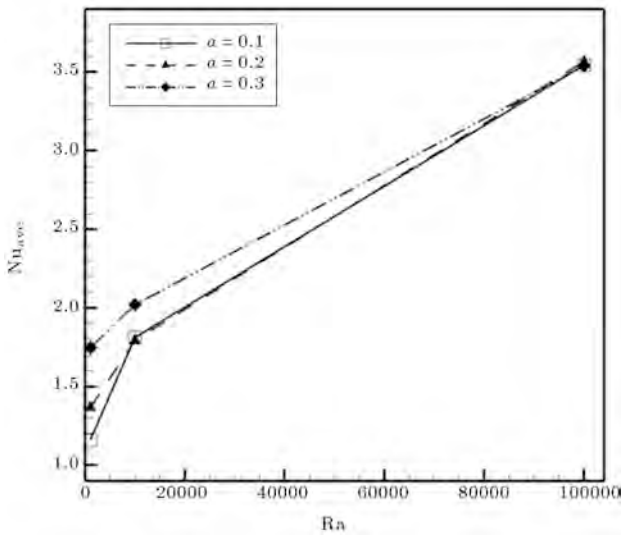

Figure 13. Effects of a and Ra on the average Nusselt number at $\gamma = 90°$, Da $= 0.1$ and, $\varepsilon = 0.5$.

wall amplitude, which inhibits the flow circulation inside the enclosure.

6. Conclusion

In this study, the effects of different governing parameters on natural convection heat transfer between an inclined hot basement roof and a cold environment, which can be approximated as an enclosure, are investigated numerically, using the Control Volume based Finite Element Method (CVFEM). The cold wall of the enclosure is assumed to mimic a sinusoidal profile with different dimensionless amplitudes. From the numerical investigation, it can be concluded that the inclination angle (γ) of the enclosure and the dimensionless amplitude of the sinusoidal wall (a) can control the parameters at different Darcy number and porosity. In addition, the effects of increasing a on the streamlines and local and average Nusselt numbers depend on the values of Rayleigh number and inclination angle of the enclosure. Moreover, the streamlines and isotherms indicate that both a and γ have an obvious effect on the formation and division of the vortices inside the enclosure, as well as the strength of flow in the upper and lower regions of the enclosure and magnitude of the local Nusselt number on the hot wall. To examine the effect of Darcy number and various values of porosity on the heat transfer and fluid flow inside the enclosure, the effects of these parameters are investigated in terms of streamlines, isotherms, local and average Nusselt numbers.

References

1. Nithiarasu, P., Seetharamu, K.N. and Sundararajan, T. "Natural convective heat transfer in a fluid saturated variable porosity medium", *Int. J. Heat Mass Transfer*, **40**(16), pp. 3955-3967 (1997).

2. Pakdee, W. and Rattanadecho, P. "Unsteady effects on natural convective heat transfer through porous media in cavity due to top surface partial convection", *Applied Thermal Engineering*, **26**(17-18), pp. 2316-2326 (2006).

3. Baytas, A.C. and Pop, I. "Natural convection in a trapezoidal enclosure filled with a porous medium", *Int. J. Eng. Sci.*, **39**(2), pp. 125-134 (2001).

4. Saidi, C., Legay, F. and Pruent, B. "Laminar flow past a sinusoidal cavity", *Int. J. Heat Mass Transfer*, **30**(4), pp. 649-660 (1987).

5. Das, P.K. and Mahmud, S. "Numerical investigation of natural convection inside a wavy enclosure", *Int. J. Therm. Sci.*, **42**(4), pp. 397-406 (2003).

6. Adjlout, L., Imine, O., Azzi, A. and Belkadi, M. "Laminar natural convection in an inclined cavity with a wavy wall", *Internat. J. Heat Mass Transfer*, **45**(10), pp. 2141-2152 (2002).

7. Mahmud, S., Das, P.K., Hyder, N. and Islam, A.K.M. "Free convection in an enclosure with vertical wavy walls", *Int. J. Therm. Sci.*, **41**(5), pp. 440-446 (2002).

8. L.S. Yao. "Natural convection along a vertical wavy surface", *J. Heat Transfer*, **105**(3), pp. 465-468 (1983).

9. Dalal, A. and Das, M.K. "Natural convection in a cavity with a wavy wall heated from below and uniformly cooled from the top and both sides", *J. Heat Transfer*, **128**(7), pp. 717-725 (2006).

10. Rostami, J. "Unsteady natural convection in an enclosure with vertical wavy walls", *Heat Mass Transfer*, **44**(9), pp. 1079-1087 (2008).

11. Rathish Kumar, B.V. "A study of free convection induced by a vertical wavy surface with heat flux in a porous enclosure", *Numer. Heat Transfer A: Appl.*, **37**(5), pp. 493-510 (2000).

12. Chen, X.B., Yu, P., Winoto, S.H. and Low, H.T. "Free convection in a porous cavity based on the Darcy-Brinkman-Forchheimer extended model", *Numer. Heat Transfer A*, **52**(?), pp. 377-397 (2007).

13. Ghasemi, E., Soleimani, S., Barari, A., Bararnia, H. and Domairry, G. "The influence of uniform suction/injection on heat transfer of MHD Hiemenz flow in porous media", *ASCE Journal of Engineering Mechanics*, **138**(1), pp. 82-88 (2012).

14. Bararnia, H., Ghasemi, E., Soleimanikutanaei, S., Barari, A and Ganji, D.D. "HPM-Padé method on natural convection of Darcian fluid about a vertical full cone embedded in porous media", *Journal of Porous Media*, **14**(6), pp. 545-553 (2011).

15. Bararnia, H., Ghasemi, E., Domairry, G. and Soleimani, S. "Behavior of micro-polar flow due to linear stretching of porous sheet with injection and suction", *Advances in Engineering Software*, **41**(6), pp. 893-897.

16. Moghimi, S.M., Domairry, G., Bararnia, H., Soleimani, S. and Ghasemi, E. "Numerical study of natural convection in an inclined L-shaped porous enclosure", *Adv. Theor. Appl. Mech.*, **5**(5), pp. 237-245 (2012).

17. Ghasemi, E., Bayat, M. and Bayat, M. "Visco-elastic MHD flow of Walters liquid b fluid and heat transfer over a non-isothermal stretching sheet", *Int. J. Phys. Scienc.*, **6**(21), pp. 5022-5039 (2011).

18. Bararnia, H., Ghasemi, E., Soleimani, S., Baraei, A. and Ganji, D.D. "HPM-Padé method on natural convection of Darcian fluid about a vertical full cone embedded in porous media", *J. Porous. Media.*, **14**, pp. 545-553 (2011).

19. Bararnia, H., Ghasemi, E., Soleimani, S., Ghotbi, A.R. and Ganji, D.D. "Solution of the Falkner-Skan wedge flow by HPM-Pade' method", *Advanc. Engineer. Softwar.*, **43**, pp. 44-52 (2012).

20. Moghimi, S.M., Domairry, G., Bararnia, H., Ghasemi, E. and Soleimani, S. "Application of homotopy analysis method to solve MHD Jeffery-Hamel flows in non-parallel walls", *Advanc. Engineer. Softwar.*, **42**, pp. 108-113 (2011).

21. Baliga, B.R. "Control-volume finite element methods for fluid flow and heat transfer", In *Advances in Numerical Heat Transfer*, **1**, W.J. Minkowycz, E.M. Sparrow, Eds., New York, Taylor & Francis., pp. 97-136 (1996).

22. Soleimani, S., Sheikholeslam, M., Ganji, D.D. and Gorji-Bandpay, M. "Natural convection heat transfer in a nanofluid filled semi-annulus enclosure", *Int. Commun. Heat Mass Transf.*, **39**(4), pp. 565-574 (2012).

23. Ghasemi, E., Soleimani, S. and Bararnia, H. "Natural convection between a circular enclosure and an elliptic cylinder using control volume based finite element method", *Int. Commu. Heat. Mass. Trans.*, **39**(8). pp. 1035-1044 (2012).

24. Voller, V.R., *Basic Control Volume Finite Element Methods for Fluids and Solids*, World Scientific Publishing Co. Pte. Ltd. 5 Tohccxxvc (2009).

25. Taeibi-Rahni, M., Ramezanizadeh, M., Ganji, D.D., Darvan, A., Ghasemi, E., Soleimani, S. and Bararnia, H. "Large-eddy simulations of three dimensional turbulent jet in a cross flow using a dynamic subgrid-scale eddy viscosity model with a global model coefficient", *Int. Commu. Heat. Mass. Trans.*, **38**(5), pp. 659-667 (2011).

26. Soleimani, S., Ganji, D.D., Gorji, M., Bararnia, H. and Ghasemi, E. "Optimal location of a pair heat source-sink in an enclosed square cavity with natural convection through PSO algorithm", *Int. Commu. Heat. Mass. Trans.*, **38**(5), pp. 652-658 (2011).

27. Taeibi-Rahni, M., Ramezanizadeh, M., Darvan, A., Ganji, D.D., Soleimani, S., Ghasemi, E. and Bararnia, H. "Large-eddy simulations of three dimensional turbulent jet in a cross flow using a dynamic subgrid-scale eddy viscosity model with a global model coefficient", *World Applied Sciences J.*, **9**(10), pp. 1191-1200 (2010).

28. Ghasemi, E., McEligot, D.M., Nolan, K., Crepeau, J., Tokuhiro, A. and Budwig, R.S. " Entropy generation in transitional boundary layer region under the influence of freestream turbulence using transitional RANS models and DNS", *Int. Comm. Heat. Mass. Transfer*, **41**, pp. 10-16 (2013).

29. Brinkmann, H.C. "On the permeability of media consisting of closely packed porous particles", *Appl. Sci. Res.*, **1**(1), pp. 81-86 (1949).

30. Lauriat, G. and Prasad, V. "Natural convection in a vertical porous cavity: a numerical study for Brinkmann-extended Darcy formulation", *Trans. ASME J. Heat Transfer*, **109**(3), pp. 295-320 (1987).

31. Al-Amiri, A.M. "Analysis of momentum and energy transfer in a liddriven cavity filled with a porous medium", *Int. J. Heat Mass Transfer*, **43**(19), pp. 3513-3527 (2000).

32. Khanafer, K., Vafai, K. and Lightstone, M. "Buoyancy-driven heat transfer enhancement in a two dimensional enclosure utilizing nanofluids", *Int. J. Heat Mass Transfer*, **46**(19), pp. 3639-3653 (2003).

33. De Vahl Davis, G. "Natural convection of air in a square cavity, a benchmark numerical solution", *Int. J. Numer. Methods Fluids*, **3**(3), pp. 249-264 (1962).

Biographies

Asskar Janalizadeh Choobasti is an Associate Professor in Civil Engineering-Geotechnical, School of

Civil Engineering at Babol University of Technology; Babol, Iran. He received his PhD in Civil Engineering-Geotechnical from Department of Civil Engineering, School of Engineering, the University of UMIST, UK. His research interests are Soil Liquefaction, Numerical Modeling.

Saman Soleimani Kutanaei received his BS in Civil Engineering at Azad Islamic University, Ghaemshahr branch. He is currently a graduate student at Babol University of Technology, Babol, Iran. His main research interests are Soil Liquefaction, numerical modeling the solidification phenomena, optimization using genetic algorithm and neural network and experimental study of new concepts in civil engineering.

Esmaiil Ghasemisahebi received his MS in Mechanical Engineering in thermo-fluid subfield at University of Idaho. He is currently a graduate student at Florida International University where he performs research on Turbulent Reacting Flows. His main research interests are computational fluid dynamics and computational physics, turbulent flow modeling, heat transfer and entropy generation.